INTERNATIONAL JOURNAL FOR NUMERICAL METHODS IN FLUIDS
Int. J. Numer. Meth. Fluids 2013; **71**:634–651
Published online 18 April 2012 in Wiley Online Library (wileyonlinelibrary.com/journal/nmf). DOI: 10.1002/fld.3676

An assessment of particle methods for approximating anisotropic dispersion

Paulo A. Herrera[1,*,†] and Roger D. Beckie[2]

[1]*Department of Civil Engineering, University of Chile, Av. Blanco Encalada 2002, Santiago, Chile 8370449*
[2]*Department of Earth and Ocean Sciences, University of British Columbia, 6339 Stores Road, Vancouver, BC, Canada V6T 1Z4*

SUMMARY

We derive a smoothed particle hydrodynamics (SPH) approximation for anisotropic dispersion that only depends upon the first derivative of the kernel function and study its numerical properties. In addition, we compare the performance of the newly derived SPH approximation versus an implementation of the particle strength exchange (PSE) method and a standard finite volume method for simulating multiple scenarios defined by different combinations of physical and numerical parameters. We show that, for regularly spaced particles, given an adequate selection of numerical parameters such as kernel function and smoothing length, the new SPH approximation is comparable with the PSE method in terms of convergence and accuracy and similar to the finite volume method. On other hand, the performance of both particle methods (SPH and PSE) decreases as the degree of disorder of the particle increases. However, we demonstrate that in these situations the accuracy and convergence properties of both particle methods can be improved by an adequate choice of some numerical parameters such as kernel core size and kernel function. Copyright © 2012 John Wiley & Sons, Ltd.

Received 23 September 2011; Revised 2 January 2012; Accepted 12 March 2012

KEY WORDS: Lagrangian; meshfree; particle method; porous media; transport; advection–diffusion

Solute transport in natural porous media is usually modeled using an advection–dispersion equation (ADE). Under normal field conditions, the transport process is advection-controlled and the resulting parabolic partial differential equation exhibits more of a hyperbolic character. On the other hand, the natural heterogeneity of geological formations results in rapid changes of the magnitude and direction of the flow velocity. Those features make the numerical solution of the resulting transport equation with traditional mesh-based methods very challenging. The numerical solution is further complicated by the fact that the dispersion coefficient that appears in the ADE is a second-order tensor with principal axes that are oriented parallel and perpendicular to the flow velocity [1], so that the spreading of a contaminant plume is anisotropic: faster in the longitudinal direction than in the transverse direction.

Particle methods offer advantages for the simulation of solute transport in natural porous media because of their natural ability to adapt to the flow velocity and to simulate advection-controlled transport without introducing numerical dispersion and artificial mixing. Thus, there has been a long dated interest in the use of particle methods to simulate solute transport in the subsurface

*Correspondence to: Paulo A. Herrera, Department of Civil Engineering, University of Chile, Av. Blanco Encalada 2002, Santiago, Chile 8370449.

†E-mail: pherrera@ing.uchile.cl

(e.g., [2] and references therein). The main challenge for the use of particle methods has been in deriving robust approximations for simulating solute dispersion, which is key to represent solute mixing and dilution.

Recent approaches to incorporate diffusion, dispersion, or viscous effects in particle simulations are based on an integral approximation of second-order derivatives [3–5]. Particle locations are used as quadrature points to discretize integral approximations of second-order derivatives. When used to simulate solute transport, these methods approximate the local dispersion operator by using concentration values at a set of scattered particles or nodes [6, 7]. The effects of dispersion are incorporated, modifying concentration values of individual particles as to simulate the result of mass exchange between neighboring particles or fluid regions. Therefore, important physical mechanisms to understand solute transport in porous media such as dilution and solute mixing can be directly simulated.

There have been two studies that have evaluated the use of particle methods on the basis of integral representations of second derivatives to simulate solute transport in natural aquifers [6, 7]. First, Zimmermann *et al*. [6] investigated the use of the particle strength exchange (PSE) method [3, 8] to simulate solute transport in homogeneous porous media considering anisotropic dispersion and uniform and nonuniform flow conditions. Their results showed that the PSE approximation provides accurate results for a set of benchmark problems if a remeshing procedure was used to control the irregular particle distribution due to the flow velocity. Later, Herrera *et al*. [7] compared a smoothed particle hydrodynamics (SPH) approximation to simulate conservative transport in heterogeneous porous media with a high-order finite volume (FV) and a hybrid method of characteristics solvers assuming isotropic dispersion only. Herrera *et al*. [7] used an SPH approximation for second derivatives, first introduced by Cleary and Monaghan [4] to simulate thermal conduction, that only involves the first derivative of the kernel in contrast to other SPH formulations for second derivatives that depend upon the second derivatives of the kernel function [9]. The formulation based on the first derivative of the kernel is less sensitive to particle disorder than the one based on the second derivatives that, in general, require a remeshing procedure to control the effect of the irregular particle distribution [9]. The results presented in [7] confirm this by showing that the SPH formulation of Cleary and Monaghan [4] without a remeshing step can be used to simulate isotropic dispersion in the presence of nonuniform velocity fields, which distort the particle distribution, while providing solutions that compare favorably with other calculated with standard numerical techniques. In addition, these results clearly show the advantages of the SPH approximation for simulating advection-dominated solute transport in heterogeneous porous media.

Another challenge for the correct simulation of reactive transport in porous media has been related to developing robust numerical algorithms (particle-based or mesh-based) to avoid numerical oscillations that plague most traditional numerical approximations of parabolic or elliptic equations that include mixed derivatives or cross-terms [10–16].

Because of the good performance of particle methods to simulate solute transport in porous media [6, 7], we are interested in extending these methods to simulate other situations and to test how they compare for simulating different scenarios. The first objective of this manuscript is to derive an SPH expression to approximate anisotropic dispersion to extend our previous work presented in [7] and to test whether this new approximation could avoid the use of a remeshing procedure required by other particle approximations [6, 9]. The second objective is to test and compare the SPH and PSE methods to simulate isotropic and anisotropic dispersion under different conditions. As reference, we also compare both particle methods versus a standard FV formulation. In particular, we are interested in understanding the convergence properties of both particle methods, the factors that control their accuracy, and their relative performance in comparison with a well-established mesh-based solver. We believe that this is the first direct comparison between the SPH and PSE methods for the simulation of dispersive processes reported in the literature. The third objective is to study the monotonicity properties of the proposed SPH and the PSE approximations for different degrees of anisotropy of the dispersion tensor, to evaluate whether they could be used in situations when numerical oscillations of the solution cannot be tolerated, for example, in reactive transport simulations.

DOI: 10.1002/fld

1. MATHEMATICAL FORMULATION

In what follows, we will focus on the numerical solution of an ADE that describes the migration of passive solutes in porous media. The Lagrangian formulation of this transport equation can be written as

$$\frac{\mathrm{d}\mathbf{r}}{\mathrm{d}t} = \mathbf{v}(\mathbf{r}, t) \tag{1}$$

$$\frac{\mathrm{d}C(\mathbf{r}, t)}{\mathrm{d}t} = \nabla \cdot (\mathbf{D}(\mathbf{r}) \nabla C(\mathbf{r}, t)) \tag{2}$$

where $\mathbf{r}$ is the position of a fluid particle, $C(\mathbf{r}, t)$ is the solute concentration [ML^{-3}], $\mathbf{D}(\mathbf{r})$ is the hydrodynamic dispersion coefficient [$\mathrm{L}^2\mathrm{T}^{-1}$], and $\mathbf{v}$ is the pore water velocity [LT^{-1}]. The first equation describes the movement of a fluid particle due to the flow velocity, whereas the second one describes the change in concentration due to hydrodynamic dispersion. In what follows, we will consider that the flow field is computed externally, and it is an input parameter for the transport simulation.

In isotropic porous media, the components of the tensor $\mathbf{D}$ are given by [1]

$$D_{ij} = (\alpha_{\mathrm{T}} |\mathbf{v}| + D^{\mathrm{m}}) \delta_{ij} + (\alpha_{\mathrm{L}} - \alpha_{\mathrm{T}}) \frac{v_i v_j}{|\mathbf{v}|} \tag{3}$$

where α_{L} and α_{T} are the longitudinal and transverse dispersivity [L], respectively, and D^{m} is the molecular diffusivity [$\mathrm{L}^2\mathrm{T}^{-1}$]. In general, the longitudinal dispersivity is at least one order of magnitude larger than the transverse dispersivity, $\alpha_{\mathrm{T}}/\alpha_{\mathrm{L}} \ll 1$.

The solution of (1) can be easily evaluated using a semi-analytical particle tracking or an explicit time integration schemes [17, 18]. Therefore, in the rest of this manuscript, we will focus our attention on the numerical solution of (2), which represents a much more challenging problem in the context of particle methods. In the next two sections, we will present two particle-based formulations to discretize (2).

2. SPH APPROXIMATION

In the standard SPH formulation, the smoothed interpolation $A_{\mathrm{S}}(\mathbf{r})$ of a variable $A(\mathbf{r})$ is defined as the integral [19, 20]

$$A_{\mathrm{S}}(\mathbf{r}) = \int A(\mathbf{r}') W(\mathbf{r} - \mathbf{r}', h) \, \mathrm{d}\mathbf{r}' \tag{4}$$

where $W(\mathbf{r} - \mathbf{r}', h)$ is a kernel function with smoothing length h that satisfies [21]

$$\int W(\mathbf{r} - \mathbf{r}', h) \, \mathrm{d}\mathbf{r}' = 1 \tag{5}$$

$$\lim_{h \to 0} W(\mathbf{r} - \mathbf{r}', h) = \delta(\mathbf{r} - \mathbf{r}') \tag{6}$$

Because of their practical advantages, spline polynomials with compact support are usually used as kernel functions [21].

The numerical approximation of the integral in (4) is evaluated as

$$A(\mathbf{r}_a) = \sum_b \frac{1}{p_b} A(\mathbf{r}_b) W(|\mathbf{r}_a - \mathbf{r}_b|) \tag{7}$$

where p_b is a measurement of the spatial particle density around $\mathbf{r}_b$. In most cases, it is approximated as

$$p_b = \sum_a W(|\mathbf{r}_a - \mathbf{r}_b|) \tag{8}$$

DOI: 10.1002/fld

When computing approximations for first-order and second-order derivatives, it is also useful to introduce the scalar function $F(\mathbf{r})$ such that the gradient of a spherically symmetric kernel can be evaluated as [4, 22]

$$\nabla W(\mathbf{r}) = \mathbf{r} F(\mathbf{r}) \tag{9}$$

2.1. SPH approximation for tensorial diffusion

To derive an SPH expression to evaluate (2), we use the following identity

$$\sum_i \sum_j \frac{\partial}{\partial x_i} D_{ij} \frac{\partial C}{\partial x_j} = \frac{1}{2} \sum_i \sum_j \left[\frac{\partial^2}{\partial x_i \partial x_j} (D_{ij} C) - C \frac{\partial^2 D_{ij}}{\partial x_i \partial x_j} + D_{ij} \frac{\partial^2 C}{\partial x_i \partial x_j} \right] \tag{10}$$

which is valid for any symmetric tensor $\mathbf{D}$. This expression is the generalization of the identity used by Jubelgas *et al*. [22] to derive an SPH approximation for thermal conduction. Second derivatives of a scalar field A can be evaluated using [23, 24]

$$\left. \frac{\partial^2 A}{\partial x_i \partial x_j} \right|_a = \sum_b \frac{1}{p_b} (A_a - A_b) F(\mathbf{r}_a - \mathbf{r}_b) \left[\Gamma \frac{(\mathbf{r}' - \mathbf{r})_i (\mathbf{r}' - \mathbf{r})_j}{|\mathbf{r}' - \mathbf{r}|^2} - \delta_{ij} \right] \tag{11}$$

where $\Gamma = 4$ in two dimensions and $\Gamma = 5$ in three dimensions.

Finally, substituting (11) into (10), we arrive at our SPH approximation for (2),

$$\frac{\mathrm{d}C_a}{\mathrm{d}t} = \frac{1}{2} \sum_b \frac{1}{p_{ab}} (C_a - C_b) F(|\mathbf{r}_a - \mathbf{r}_b|) \mathcal{D}(\mathbf{r}_a, \mathbf{r}_b) \tag{12}$$

with

$$\begin{aligned} \mathcal{D}(\mathbf{r}_a, \mathbf{r}_b) &= \sum_i \sum_j (D^a_{ij} + D^b_{ij}) \left[4 \frac{(\mathbf{r}_b - \mathbf{r}_a)_i (\mathbf{r}_b - \mathbf{r}_a)_j}{|\mathbf{r}_b - \mathbf{r}_a|^2} - \delta_{ij} \right] \\ &= \sum_i \sum_j D^{ab}_{ij} \Theta_{ij} (\mathbf{r}_b - \mathbf{r}_a) \end{aligned} \tag{13}$$

where $\mathbf{D}^a$ is the dispersion tensor at position $\mathbf{r}_a$, and we have replaced the density p_b by a symmetric expression $p_{ab} = f(p_a, p_b)$, for example, the arithmetic average of p_a and p_b, to ensure a symmetric approximation [7]. This expression reduces to the standard SPH approximation for diffusion [7, 25] or thermal conduction [4, 22], if $\mathbf{D} = D\mathbf{I}$, where $\mathbf{I}$ is the identity matrix. In simulations that consider variable coefficients, the term $D^{ab}_{ij} = (D^b_{ij} + D^a_{ij})$ can be substituted by an effective coefficient of the form $D^{ab}_{ij} = 2D^a_{ij} D^b_{ij} / (D^a_{ij} + D^b_{ij})$, which has given more robust results in thermal conduction simulations [4, 22].

The approximation (12) has two sources of error. First, the SPH integral interpolant (4) introduces an error that grows with the smoothing length. Second, the numerical discretization of the integral introduces an error that depends on the number and position of the particles that contribute to the summation in (7). This source of error is related to the ratio between the average number of particles per kernel smoothing length $\gamma = h/\Delta x$, where Δx is the average particle spacing. In general, a larger number of particles per kernel support volume (larger γ) and result in a better approximation of the integral. However, the use of large γ values while controlling h to minimize the interpolant error requires an increasingly small particle spacing and hence a large number of particles. Therefore, one must make a trade-off between γ and h to obtain reasonable error while controlling the number of particles and computational effort [4].

2.2. Monotonicity

It is well known that traditional numerical approximations of parabolic or elliptic equations of the form (2) that consider the off-diagonal terms of the dispersion tensor do not satisfy the monotonicity properties of the solution (e.g., see [26] and references therein for details). The development

DOI: 10.1002/fld

of numerical approximations that overcome those numerical issues is still the object of intense research [11, 13, 14, 16, 27]. Here, we study the monotonicity properties of the SPH approximation derived previously.

First, we notice that (12) has the form

$$\frac{\mathrm{d}C_i}{\mathrm{d}t} = \sum_{j \neq i} \beta_{ij}(C_j - C_i) = \sum_j \hat{\beta}_{ij} C_j \tag{14}$$

with $\hat{\beta}_{ii} = -\sum_{j \neq i} \beta_{ij}$; thus, $\sum_j \hat{\beta}_{ij} = 0$.

Then, we can use the local extremum diminishing (LED) criteria [28] to study the monotonicity of this numerical discretization. A numerical approximation such as (14) satisfies the LED criteria if $\beta_{ij} \geqslant 0,\ i \neq j$ [29], which is a sufficient condition to obtain monotonic solutions, as can be easily demonstrated by the following rationale. If the concentration at node i, C_i, is a minimum, the temporal derivative of the concentration at that node is positive or zero. Therefore, a minimum concentration can only increase or stay constant. Similar arguments can be used to prove that a maximum value cannot increase.

In the case of (12), we have that

$$\beta_{ab} = -\frac{1}{2}\frac{1}{p_{ab}} F(|\mathbf{r}_a - \mathbf{r}_b|)\mathcal{D}(\mathbf{r}_a, \mathbf{r}_b) \quad a \neq b \tag{15}$$

with $F(r) \leqslant 0$ because of the kernel properties.

Then, the LED criteria requires that $\mathcal{D}(\mathbf{r}_a, \mathbf{r}_b) \geqslant 0$. This condition cannot be demonstrated for the general case of an irregular node distribution or nonuniform flow, but it can be studied for the simple case of equispaced nodes in a square lattice in a uniform flow field. To make the analysis simpler, we use a polar coordinate system such that θ is the angle formed by the vector connecting two nodes located at $\mathbf{r}_a$ and $\mathbf{r}_b$ and the x-axis. Then, we obtain that $\Theta_{xx} = 4\cos^2\theta - 1$, $\Theta_{yy} = 4\sin^2\theta - 1$, and $\Theta_{xy} = 4\sin\theta\cos\theta$. In a square lattice, $\theta = [0,\ \pi/4,\ \pi/2]$ or a multiple of those numbers. For $\theta = 0$ or $\theta = \pi/2$, there is only one term that is not zero, and it is positive. If $\theta = n\pi/4$ with n integer, we have that $\mathcal{D}(\mathbf{r}_a, \mathbf{r}_b) = D^{ab}_{xx} + D^{ab}_{yy} + 4D^{ab}_{xy}$, which can be positive or negative because of the change in sign of D_{xx}, D_{yy}, and D_{xy} with the flow orientation according to (3). Figure 1 shows the value of $\mathcal{D}(\mathbf{r}_a, \mathbf{r}_b)$ as a function of the velocity direction for $\theta = n\pi/4$. This figure shows that it is possible that $\mathcal{D}(\mathbf{r}_a, \mathbf{r}_b) \not\geqslant 0$ depending upon the flow orientation. This implies that the SPH discretization with nodes distributed in a square lattice does not satisfy the LED criteria and that the numerical solution of (12) might exhibit negative concentrations depending upon the flow orientation. This is confirmed by the results of numerical simulations presented later.

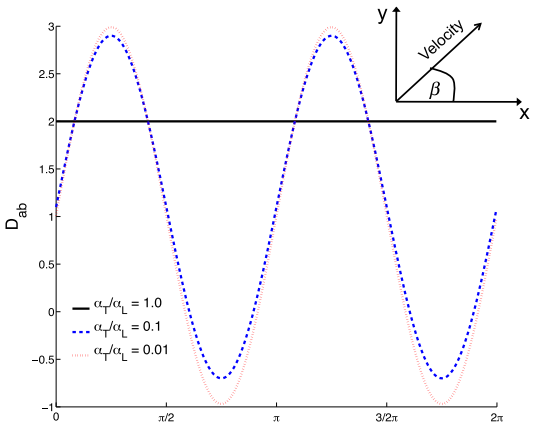

Figure 1. Coefficient $\mathcal{D}(\mathbf{r}_a, \mathbf{r}_b) = D_{xx} + D_{yy} + 4D_{xy}$ for $|\mathbf{v}| = 1$ and such that $\mathbf{r} = \mathbf{r}_b - \mathbf{r}_a$ forms an angle of 45° with the x-axis as function of the angle β formed by the flow velocity and the x-axis.

DOI: 10.1002/fld

3. PARTICLE STRENGTH EXCHANGE APPROXIMATION

The PSE discretization of (2) is also based on an integral approximation [3]. Here, we present the approximation for anisotropic diffusion derived in [8] and used in [6] that reads

$$\frac{\mathrm{d}C_a}{\mathrm{d}t} = \frac{(\Delta x)^2}{\varepsilon^6} \sum_b \left[(C_b - C_a) K(r_{ab}, \varepsilon) \sum_i \sum_j M_{ij}(\mathbf{r}_a, \mathbf{r}_b)(\mathbf{r}_a - \mathbf{r}_b)_i (\mathbf{r}_a - \mathbf{r}_b)_j \right] \tag{16}$$

where Δx is the representative inter-particle spacing, $K(r_{ab}, \varepsilon)$ is a cutoff function that satisfies the so-called moment conditions, ε is known as the core size that defines the size of the area of influence of each particle, and the components of the matrix $\mathbf{M}(\mathbf{r}_a, \mathbf{r}_b)$ are given by

$$M_{ij}(\mathbf{r}_a, \mathbf{r}_b) = \frac{1}{2}(m_{ij}(\mathbf{r}_a) + m_{ij}(\mathbf{r}_b)) \tag{17}$$

where

$$\mathbf{m}(\mathbf{r}) = \mathbf{D}(\mathbf{r}) - \frac{1}{4}\mathrm{tr}(\mathbf{D}(\mathbf{r}))\mathbf{I} \tag{18}$$

with $\mathrm{tr}(\mathbf{D}) = \sum_i D_{ii}$. Zimmermann *et al*. [6] provided expressions for second-order, fourth-order, and sixth-order cutoff kernels. Eldredge *et al*. [5] provided expressions to compute kernels that are up to eighth order in one and two dimensions and discussed their properties.

The same analysis used in the previous section to study the monotonicity properties of the SPH approximation can be used to demonstrate that (16) does not guarantee the monotonicity of the solution when the full dispersion tensor is considered [8], which was also confirmed through numerical simulations by Zimmermann *et al*. [6].

Because of the similarities between the SPH and the PSE methods, it is possible to establish a direct parallel between the kernel and the cutoff functions and between the smoothing length and core size in SPH and PSE, respectively. In the rest of this manuscript, we will use the terms *kernel* or *cutoff function* to refer to the function K and the terms *core size* or *smoothing length* to refer to ε. We will also use W to refer to the cutoff K and h instead of ε to refer to the core size whenever such change helps to simplify notation.

4. NUMERICAL TESTS

4.1. Setup

We next evaluate the accuracy of our SPH anisotropic dispersion approximation and the PSE method from [6, 8]. We simulate the instantaneous release of a solute mass ΔM in an unbounded two-dimensional domain with a temporally and spatially constant velocity to study the accuracy and controls on error of the SPH and PSE approximations. We also use a standard nine-point FV scheme in a Cartesian grid [26, 30] to define a base case to compare the relative performance of both particle methods. A similar problem has been previously used to study the convergence properties of the PSE [6] and diffusion velocity methods [31].

Because we are interested in numerical approximations of dispersion, we simplify the problem and neglect the contribution of advection. In this case, the transport process depends on the flow only through the relation of the dispersion tensor and the flow velocity given by (3). Because advection can be easily incorporated within a particle framework without introducing additional errors, the results of our analysis can be directly extrapolated to more realistic situations.

The analytical solution for the solute concentration as function of position and time is given by [32]

$$c(\mathbf{x}, t) = \frac{C1}{C4} \exp\left(\frac{-X^2(2tD_{yy} + w^2) - Y^2(2tD_{xx} + w^2) + 4XYtD_{xy}}{8t^2C2 + 4w^2tC3 + 2w^4} \right) \tag{19}$$

where $X = x - x_0$ and $Y = y - y_0$ (x_0, y_0) is the position of the initial solute release, w is a measure of the size of the initial input, the constant $C1$ is related to the initial mass ΔM, and the other

DOI: 10.1002/fld

Table I. Parameters used in numerical tests.

Parameter	Symbol	Value	Unit
Released mass	ΔM	10^7	g
Initial plume width	w	44	m
Maximum initial concentration	C_0	320	mg/L
Length numerical domain	L	2000	m
Longitudinal dispersivity	α_{L}	10	m
Time step	Δt	1	day
Total time	T	300	day

constants are $C2 = D_{xx}D_{yy} - D_{xy}^2$, $C3 = D_{xx} + D_{yy}$, and $C4 = \sqrt{4t^2C2 + 2twC3 + w^4}$. To simplify the presentation of the results, we choose $C1 = C_0w^2$ such that the maximum initial concentration is equal to C_0. Table I shows a summary of the parameters used to set up the test problem.

The three solutions are computed using an explicit fourth-order Runge–Kutta solver to integrate in time. The use of an explicit solver imposes restrictions on the size of the time step to obtain stable solutions. The three methods have stability limits of the form

$$\Delta t \leqslant C_T \frac{\Delta^2}{D_{xx} + D_{yy}} \tag{20}$$

where Δ is the grid size for the FV, core size for the PSE [6], and smoothing length for the SPH approximations [4], respectively. The constant C_T is equal to 0.5 for the FV approximation, and it depends upon the kernel or cutoff functions for the SPH and PSE. Higher-order cutoff functions result in slightly more restrictive stability conditions, for example, Zimmermann *et al*. [6] found that $C_T \approx 2.5$ and $C_T \approx 1.2$ for second-order and fourth-order cutoff functions, respectively. Additionally, the stability limits of both particle methods depend upon the particle distribution. We found through numerical experiments that the SPH solution is stable if $C_T = 0.1$ and use this value to compute a time step that satisfies the stability restrictions of three methods for the case of equispaced particles.

The PSE and SPH approximations require that the area of influence or support of particles overlap. Thus, one must use a core size for PSE or smoothing length for SPH that is larger than the average particle spacing. Additionally, the error of the solution given by both methods depends upon the ratio of the smoothing length to the average particle spacing. In our simulations, we used different ratios to test the influence of that parameter on the error of the solution. On the other hand, higher-order kernels and cutoff functions have larger support volume as shown in Figure 2, which results in larger areas of influence and number of neighboring particles for a given smoothing length or core size.

Efficient implementations of the PSE and SPH solvers require a fast algorithm to identify near neighbor particles. The SPH implementation is based on kernels that have compact support, so a particle interacts only with particles that are within the kernel support volume. In that case, it is easy to use a background grid to classify particles in space. The cell size of that grid is related to the kernel smoothing length such that neighboring particles are always, at most, one cell apart [33]. Kernels used in the PSE approximation are modified Gaussian functions that have infinite support. Therefore, in theory, all particles interact with each other. However, PSE kernels fall rapidly with distance, and one can assume that they have an effective compact support that is few times the core size as shown in Figure 2. In our implementation, we have assumed that the effective compact support of the PSE kernels is equal to five times the kernel core size, and we have applied the same strategy as in SPH to search for neighbor particles.

4.2. Simulation cases

To test the performance of the three numerical methods, we define different scenarios on the basis of the values of parameters such as dispersivity ratio ($\alpha_{\mathrm{T}}/\alpha_{\mathrm{L}}$), smoothing length over particle spacing

DOI: 10.1002/fld

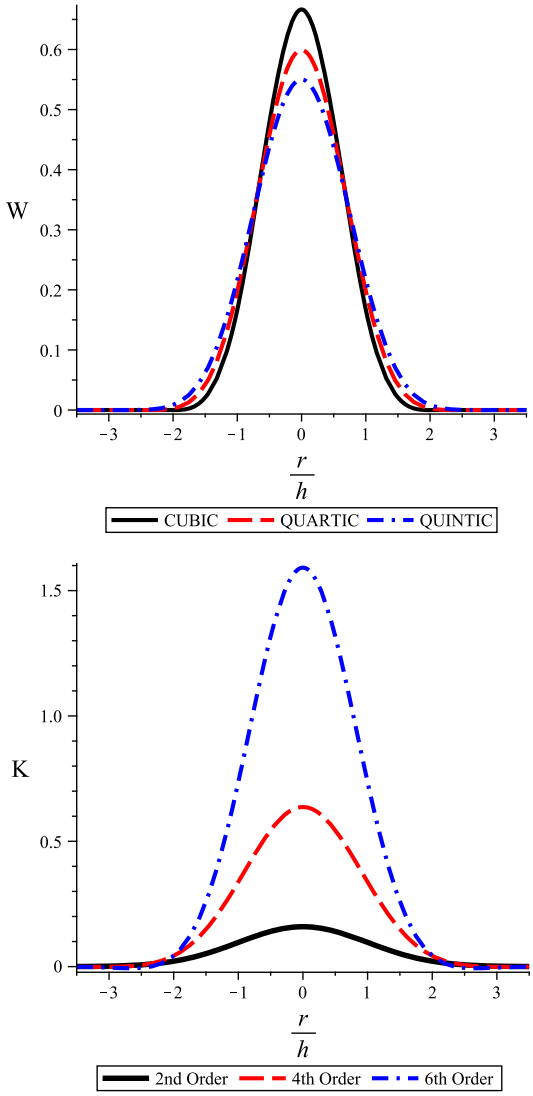

Figure 2. Cubic, quartic, and quintic SPH kernels, W, with finite compact support [34] and second-order, fourth-order, and sixth-order cutoff functions, K, used in PSE simulations [6] as function of the ratio between distance and kernel core size or smoothing length, h.

$(h/\Delta x)$, velocity direction (angle β), or SPH kernel or PSE cutoff function. The range of values of those parameters are similar to the ones used in previous studies or were selected on the basis of reasonable physical assumptions. For example, we use $\alpha_{\mathrm{T}}/\alpha_{\mathrm{L}}$ in the range $[0.001, 1.0]$ with $\alpha_{\mathrm{L}} = 10\,\mathrm{m}$ and $\beta = [0°, 45°, 53°]$, which are similar to the values reported in [6, 31]. We use values for $h/\Delta x$ and $4\varepsilon/\Delta x$ in the range $[1.0, 1.6]$, which is similar to values used in other numerical studies to study the convergence properties of the SPH approximation for thermal conduction [4] and PSE for solute dispersion [6].

We define a set of runs with different numbers of cells or particles as summarized in Table II to study the convergence of the three methods with respect to the particle or grid spacing. To assign the position of particles and cells, we assume a large square domain with side L. We assign the same number of particles and cells in each direction, N_{c}, for simulations that consider equispaced particles. For simulations that consider random or quasi-random particle distributions, the total number of particles, N, is calculated such that the average number of particles in each direction is equal to N_{c}. To measure the accuracy of the numerical solutions, we compute the errors $E_2 = \sqrt{\sum_j e_j^2/N}$

DOI: 10.1002/fld

Table II. Definition of different runs used to study convergence properties according to number of cells or average number of particles in each direction, N_c, and grid or average particle spacing, Δx.

Run	N_c	Δx
R1	40	50.0
R2	60	33.3
R3	80	25.0
R4	100	20.0
R5	120	16.7
R6	140	14.3
R7	160	12.5

and $E_\infty = \max(|e_j|)$, where e_j is the difference between analytical and numerical solutions at node j. For some simulations, we also look at the temporal evolution of the difference between the maximum concentration values of the numerical and analytical solutions. In the discussion that follows, we report errors after 200 time steps and flow direction given by $\beta = 45°$ unless explicitly indicated.

4.3. Equispaced particles

We first consider the case of equispaced particles in a square lattice. This scenario is useful because it allows the direct comparison of the particle methods and the FV approximation. Besides, the accuracy of both particle methods is expected to be optimal for this configuration; thus, the results of this section provide the best case estimate of the error of the SPH and PSE methods.

Unless explicitly specified, all the results reported for equispaced particles are computed using a cubic spline SPH kernel and second-order PSE cutoff functions.

4.3.1. Effect of particle spacing. Figure 3 shows the error E_2 versus the particle or grid spacing. For isotropic dispersion ($\alpha_T/\alpha_L = 1.0$), the convergence rate of the three methods is similar, but the mesh-based FV approximation has, on average, an error that is one order of magnitude smaller than the SPH approximation and almost two orders of magnitude smaller than the PSE approximation for the range of particle or grid spacing considered.

For $\alpha_T/\alpha_L = 0.01$ (anisotropic case), the analysis is more complicated. For all the cases, the mesh-based FV solver is more accurate than both particle methods, but the difference is smaller than for the isotropic case. The PSE and FV methods exhibit good convergence in all cases, whereas the SPH approximation is very sensitive to the ratio $h/\Delta x$. The SPH solution converges much faster for larger number of particles per kernel support volume (larger $h/\Delta x$). Nevertheless, the convergence rate of the SPH solution for small Δx is lower than for the other two methods.

4.3.2. Maximum concentrations. Figure 4 shows the difference between the maximum concentration values of the analytical and numerical solutions as function of the number of time steps. For the isotropic and anisotropic cases, the difference increases at early time until reaching a maximum value. For later times, as the initial plume smooths out, the error decreases to an asymptotic value. The SPH solution with $h/\Delta x = 1.2$ is the exception to this pattern because the error grows unboundedly with time. The difference between the numerical and the analytical solutions after 300 time steps is less than 1% for the FV and the best SPH run and around 1% for the PSE solution.

4.3.3. Negative concentrations. Figure 5 shows a comparison of the analytical and numerical solutions after 300 days for run R7 and $\alpha_T/\alpha_L = 0.01$. The three numerical solutions are similar to the analytical solution; however, they exhibit negative concentrations in bands that tend to be aligned with the main direction of the flow. Minimum simulated concentration values are $-1.8 \cdot 10^{-2}$ mg/L for FV, $-6.9 \cdot 10^{-4}$ mg/L for SPH, and $-3.2 \cdot 10^{-1}$ mg/L for PSE.

DOI: 10.1002/fld

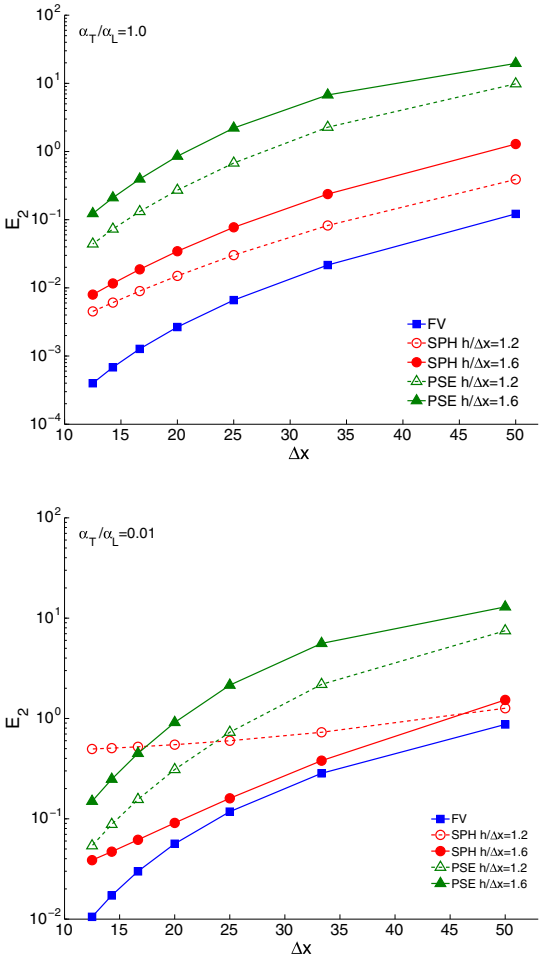

Figure 3. Error E_2 as function of particle spacing for equispaced particles and grid spacing for FV solution.

4.3.4. Effect of ratio between smoothing length and particle spacing. As discussed previously, the error of the SPH approximation for the integral in (4) depends upon the number of particles per support volume, that is, $\gamma = h/\Delta x$. Previous numerical studies have shown that the SPH approximation for scalar diffusion (isotropic case) provides accurate results even for small values of γ in the case of reasonably distributed particles [4]. On the other hand, the stability of the PSE approximation requires that particles overlap, that is, the core size must be always larger than the representative particle spacing. However, the accuracy of the approximation decreases as the core size increases; thus, it provides optimal solutions for small h that satisfy $h/\Delta x > 1$. Figure 6 shows the errors E_2 for run R6 of the SPH and PSE solutions as function of γ. We observe that, as expected, the error of the PSE solution increases monotonically with γ for the isotropic and anisotropic cases. In contrast, the SPH solution exhibits a more interesting behavior. The error of the SPH solution for the anisotropic case decreases with γ, which indicates that the error of the integral approximation controls the overall error in that case.

4.3.5. Effect of anisotropy ratio. Figure 7 shows error E_2 versus the anisotropy ratio for run R7. The error of the SPH and FV approximations is larger for smaller α_T/α_L ratio, whereas the error of the PSE method is almost constant for the range of dispersivity ratios considered. The FV approximation has the smallest error in all the cases, whereas the PSE solution is more accurate than the SPH solution for all the situations that consider anisotropic dispersion (i.e., $\alpha_T/\alpha_L \neq 1$). We note that these results consider $\gamma = 1.2$ and that according to our previous discussion, one would expect

DOI: 10.1002/fld

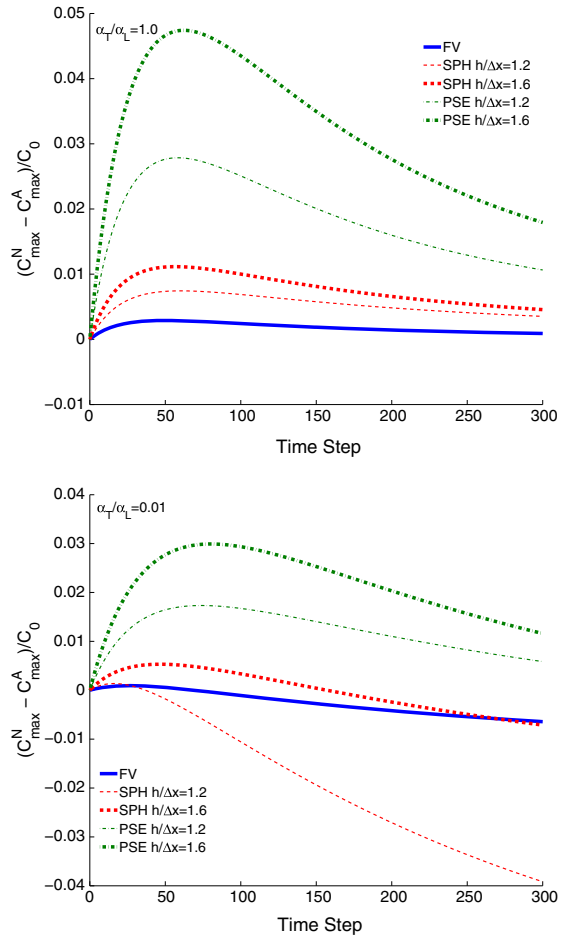

Figure 4. Difference between maximum concentration values of numerical and analytical solutions as function of time for equispaced particles and run R7. Top and bottom plots show results for the isotropic and anisotropic cases, respectively.

that the SPH solution would behave better if a larger γ is used. However, the results of our simulations indicate that the trend of increasing error for larger anisotropy ratios of the SPH and FV methods is independent of the other parameters considered in this study.

4.3.6. Effect of kernel function. Table III presents a summary of the E_2 error for run R5 for scenarios that consider different SPH kernels and PSE cutoff functions. For the isotropic case, the use of higher-order SPH kernels does not have a clear impact on the accuracy of the solution, whereas the use of higher-order PSE cutoff functions results in smaller errors. In particular, the difference between the second-order and the fourth-order cutoff functions is quite important, and it confirms that the error of the PSE approximation can be effectively controlled using higher-order cutoff functions as discussed by Eldredge *et al*. [5]. For the anisotropic case, the use of higher-order SPH kernels improves the solution, but the effect is less important than the one observed using different cutoff functions in the PSE case. Moreover, the use of higher-order cutoff functions improves the PSE approximation and makes it more accurate than the FV method for the anisotropic case.

One would expect that higher-order polynomials used as SPH kernels have the advantage of smoother derivatives, which in combination with the increased size of the support volume, would decrease the sensitivity of the kernel to the degree of particle disorder [34]. However, the results of our simulations show that the use of higher-order kernels does not provide a significant improvement of the numerical solution when particles are equispaced.

DOI: 10.1002/fld

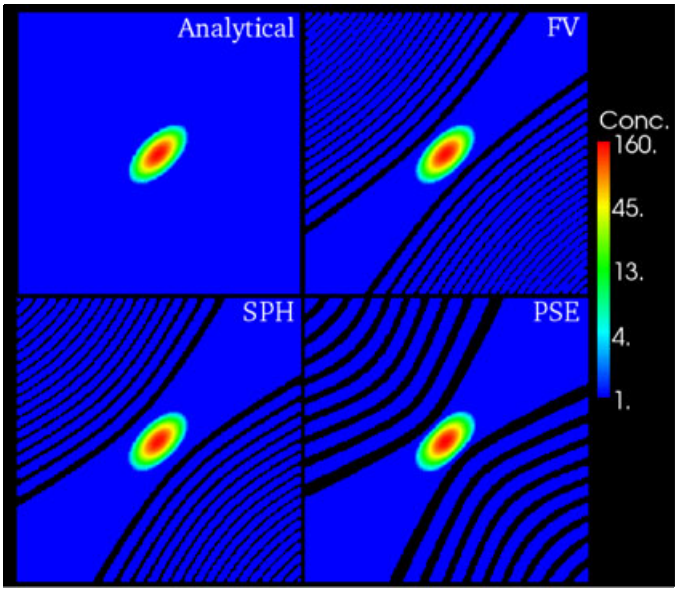

Figure 5. Concentration distribution after 300 days for run R7, $\alpha_T/\alpha_L = 0.01$, and $\beta = 45°$. All three methods exhibit negative concentrations (dark bands). Minimum concentration values are $-1.8 \cdot 10^{-2}$ for FV, $-6.9 \cdot 10^{-4}$ for SPH, and $-3.2 \cdot 10^{-1}$ for PSE. Concentration values are expressed as mg/L.

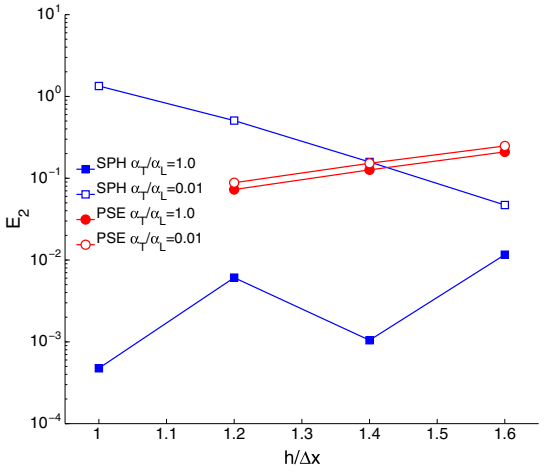

Figure 6. Error E_2 for run R6 versus the ratio between smoothing length or core size and particle spacing, $\gamma = h/\Delta x$.

4.3.7. Effect of velocity orientation. It is well known that the error of numerical mesh-based methods used to solve (2) that include the off-diagonal terms of the dispersion tensor exhibits numerical artifacts that depend upon the flow orientation with respect to the grid axes [26]. Therefore, it is interesting to test if the error of the two particle methods changes for different flow orientations. Table IV summarizes the results for run R6, assuming different flow orientations. As expected, all three methods are not sensitive to the flow direction for the isotropic case. However, for the anisotropic case, the mesh-based FV method exhibits differences of up to two orders of magnitude in the E_2 error depending upon the flow direction. The error of the SPH solution also depends upon the flow direction, but it only shows small differences for different velocity directions. On the other hand, the error of the PSE solution is almost independent of the flow direction.

DOI: 10.1002/fld

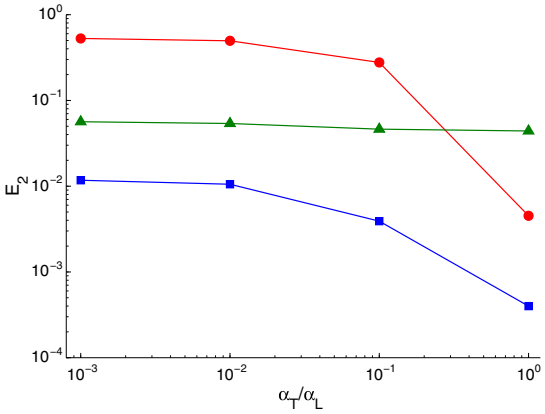

Figure 7. Error E_2 as function of the anisotropy ratio α_T/α_L for run R7 and $h/\Delta x = 1.2$ for FV (squares), PSE (triangles), and SPH (circles) solutions.

Table III. Error of the SPH and PSE numerical solutions divided by the error of the FV solution for run R5 and $h/\Delta\ x\ =\ 1.2$ considering different SPH kernels and PSE cutoff functions.

	SPH			PSE		
α_T/α_L	Kernel	E_2	E_∞	Kernel	E_2	E_∞
1	Cubic	7.0	2.7	second order	103.4	11.1
1	Quartic	4.1	2.1	fourth order	4.1	2.1
1	Quintic	7.6	2.9	sixth order	2.6	1.5
0.01	Cubic	17.4	3.9	second order	5.2	2.5
0.01	Quartic	7.1	2.6	fourth order	0.2	0.5
0.01	Quintic	4.7	2.2	sixth order	0.1	0.3

Table IV. Error versus flow velocity direction for run R6 and $h/\Delta x = 1.2$.

		SPH		PSE		FV	
α_T/α_L	β°	E_2	E_∞	E_2	E_∞	E_2	E_∞
1	45	0.0061	1.8051	0.0728	6.6221	0.0007	0.5964
1	0	0.0061	1.8051	0.0728	6.6221	0.0007	0.5964
1	53	0.0061	1.8051	0.0728	6.6221	0.0007	0.5964
0.01	45	0.5062	10.4855	0.0880	5.1519	0.0172	2.1333
0.01	0	0.6919	14.9257	0.0880	5.0957	0.0006	0.5552
0.01	53	0.4495	9.7445	0.0880	5.2464	0.0154	1.9997

4.4. Irregularly spaced particles

It is well known that the accuracy and stability of the PSE and SPH methods depend upon the spatial distribution of particles [4,6,9]. In general, at the beginning of a simulation, particles are distributed in a uniform fashion, for example, rectangular lattice. As particles move carried by the flow, high velocity gradients result in the distortion of the initial regular distribution as shown in Figure 8. This figure shows a simulated flow velocity field in a heterogeneous porus media, where large contrasts in hydraulic conductivity produce large variations of the direction and magnitude of the flow velocity. Although the initial particle distribution is disturbed because of the nonuniform velocity field, the continuity property of the flow prevents particles from moving randomly and the particle set maintains some regularity [24].

To evaluate the effect of the particle disorder on the accuracy and stability of the SPH and PSE solutions, we set up a set of simulations that evaluate the numerical solution using randomly and

DOI: 10.1002/fld

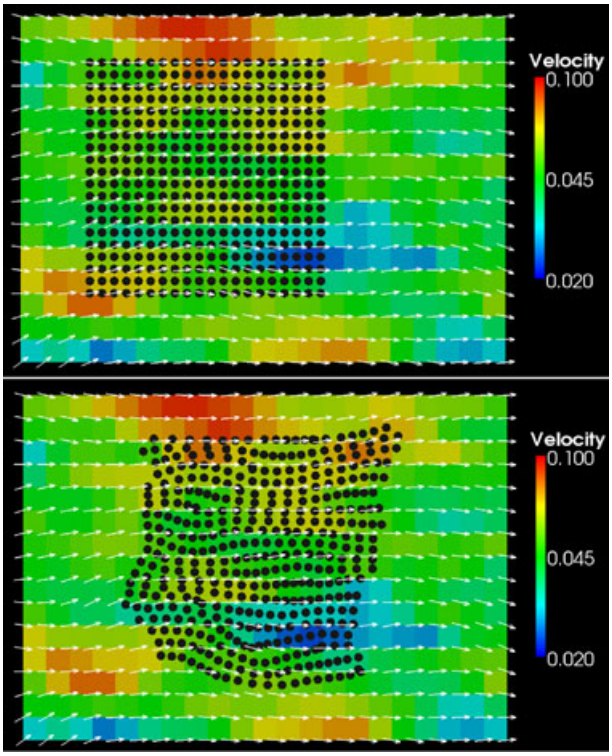

Figure 8. Particle distortion due to flow velocity. High gradients in fluid velocity (arrows) result in distortion of the initial (top figure) regular particle distribution (black circles). However, the continuity property of the flow prevents that particles become randomly distributed after some time since the beginning of the simulation (bottom figure).

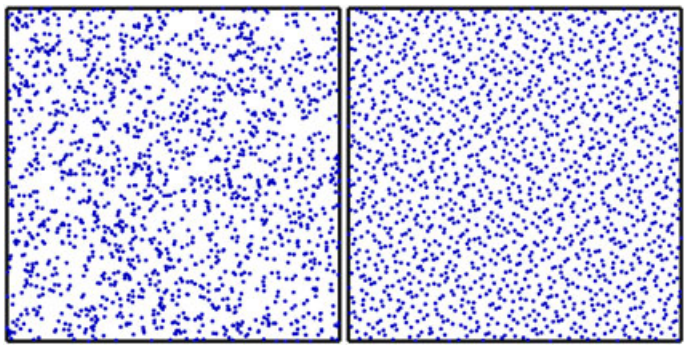

Figure 9. Particle locations for run R1 considering random (left) and quasi-random (right) distributions. The random distribution has large contrasts in particle density, whereas the quasi-random distribution has an irregular but uniform spatial particle density.

quasi-randomly distributed particles. An example of the difference between the distributions is shown in Figure 9. A random distribution results in large contrasts in the spatial density of particles in different areas of the domain. On the other hand, a quasi-random distribution results in an irregular but uniform spatial particle density. On the basis of our experience, particle distributions as result of real flow fields fall between these two extreme cases. Therefore, simulations that consider these two spatial distributions allow us to estimate upper and lower bounds for the performance of the PSE and SPH approximations for more realistic simulations.

For the simulations that consider irregularly distributed particles, we used a cubic SPH kernel and a sixth-order PSE cutoff function. The decision to use these kernel functions was based on the

DOI: 10.1002/fld

results summarized in Table III, which indicate that the impact of using different cutoff functions on the PSE solution is significant. On the other hand, the effect of the use of different kernel functions on the quality of the SPH solutions seems limited; therefore, we decided to continue using the cubic spline kernel for this new set of simulations. Despite this explanation, it is important to highlight that the comparison between the PSE and the SPH solutions presented in this section is a worst-case scenario for the SPH approximation, because better results could be achieved by using higher-order kernels.

4.4.1. Isotropic case. Figure 10 shows the error E_2 versus the average particle spacing for the same scenario but different particle spatial distribution. As seen by the slope of the curves in Figure 10, the convergence rate of the two methods decreases as particles become more disordered. Both methods converge very slowly and in a nonmonotonic fashion for the case of randomly distributed particles. It is interesting to notice that although a larger ratio $h/\Delta x$ results in a larger error for the case of equispaced particles, it actually helps in controlling the error in the case of random and quasi-random particle distributions. Overall, the PSE method is less sensitive to the disorder of the nodes than the SPH approximation.

4.4.2. Anisotropic case. Both particle approximations proved to be much more sensitive to particle disorder when simulating anisotropic dispersion than for the isotropic case. SPH simulations with random and quasi-random distributions and $h/\Delta x = 1.2$ became unstable after a few time steps.

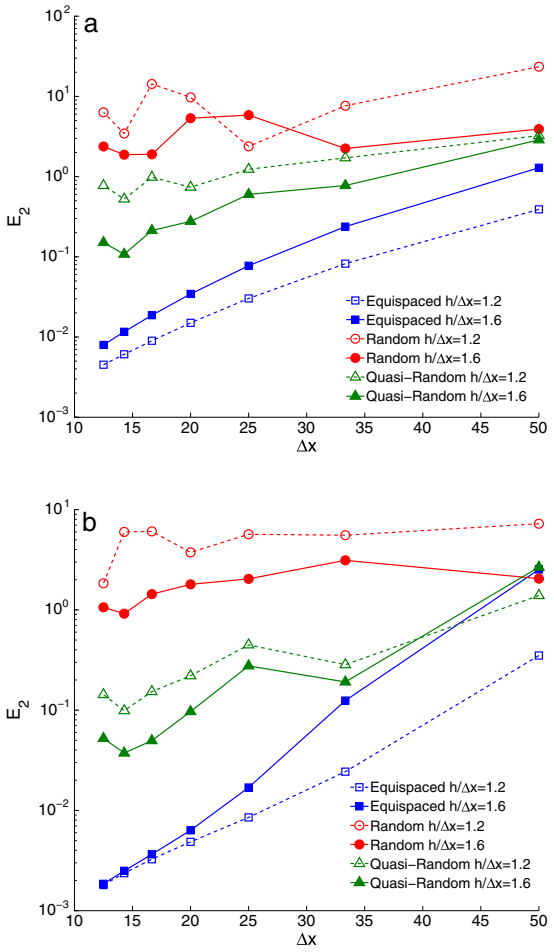

Figure 10. E_2 error of (a) SPH and (b) PSE numerical solutions versus average particle spacing for $\alpha_T/\alpha_L = 1.0$ using equispaced, random, and quasi-random particle distributions.

DOI: 10.1002/fld

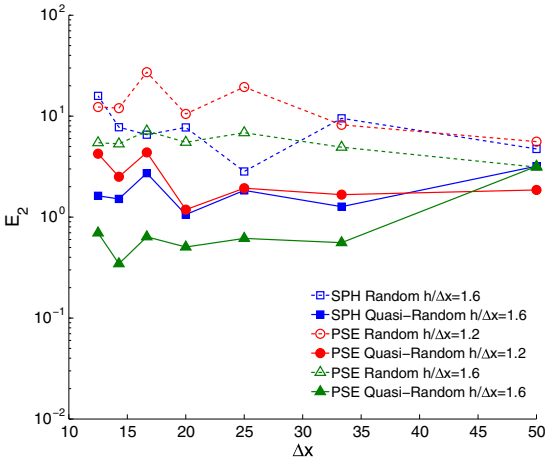

Figure 11. Error as function of average particle spacing for $\alpha_T/\alpha_L = 0.01$ using randomly and quasi-randomly distributed particles.

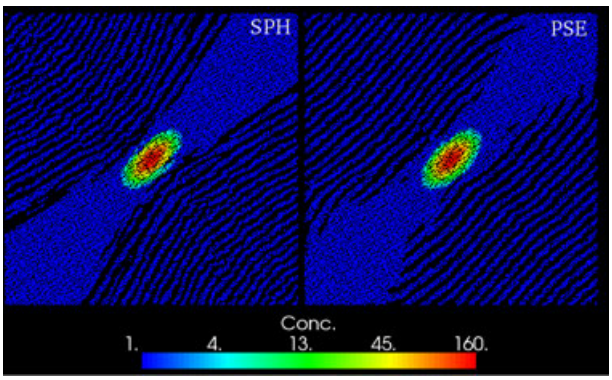

Figure 12. Concentration distribution after 300 time steps for run R7, $\alpha_T/\alpha_L = 0.01$ and quasi-randomly distributed particles. Dark bands indicate areas of negative concentrations. Minimum concentration values are −16.86 for SPH and −0.28 for PSE. Concentration values are expressed as mg/L.

For the other scenarios, the errors of both methods stay almost constant as the average particle spacing decreases, as shown in Figure 11. The use of larger smoothing lengths or core sizes results in lower errors, but it does not significantly improve the convergence rate of the numerical approximations.

Figure 12 shows the concentration field at the end of the simulation for run R7 and quasi-randomly distributed particles. Both solutions exhibit negative concentrations (dark bands) that, as for equispaced particles, are located in regions almost parallel to the flow direction. Although the maximum magnitude of the negative values in the PSE solution (−0.28) is very similar to the one observed for equispaced particles (−0.32), it is five orders of magnitude larger for the SPH solution, −16.86 for quasi-random, and $-6.9 \cdot 10^{-4}$ for equispaced particles. This may indicate that both solutions become unstable.

5. CONCLUSIONS

We derived an SPH approximation for anisotropic dispersion that only depends upon the first derivative of the kernel function. We studied some of its properties analytically and through numerical simulations. In addition, we compared the performance of the newly derived SPH approximation versus another particle method (PSE) and a standard FV scheme for the simulation of isotropic and anisotropic dispersion considering multiple scenarios defined by different combinations of physical and numerical parameters.

DOI: 10.1002/fld

The analytical and numerical results presented previously show that scenarios that include tensorial dispersion are troublesome for any of the three numerical methods tested (SPH, PSE, and FV). In particular, numerical solutions for SPH and FV simulations that include tensorial dispersion exhibit larger error and lower convergence rate than scenarios that only consider isotropic dispersion. The effect of the anisotropy ratio on the error of the PSE solution is more limited; even in some cases, PSE solutions considering anisotropic dispersion have lower error than for the equivalent scenario with isotropic dispersion. However, the numerical solutions computed with any of the three methods exhibit artificial oscillations and negative concentrations if the off-diagonal terms of the dispersion tensor are nonzero. These numerical oscillations could be particularly troublesome if these methods are used to solve nonlinear transport equations, for example, multiphase flow or reactive transport. In that case, oscillations could be amplified by nonlinear terms. We conclude that this last point represents an obstacle for the use of this kind of methods for simulations that include nonlinear terms and where the anisotropic nature of the dispersion tensor cannot be neglected.

For equispaced particles, the convergence rate of both particle methods is similar to that of the standard nine-point FV scheme. However, in contrast to the FV scheme, the convergence rate and the overall quality of the SPH and PSE methods does not only depend on the number of particles or average particle spacing used but also on other additional parameters such as kernel function and smoothing length. Because of the large number of combinations of numerical parameters that are possible, it is difficult to make an absolute statement with respect to the relative performance of both particle methods as discussed in detail in Section 4.2. We conclude that these results should motivate further numerical studies to guide the selection of the numerical parameters that are required in particle simulations.

The spatial distribution of particles is the most important factor that controls the accuracy of the numerical solutions computed with the PSE or SPH approximations. The accuracy of the solution decreased as the degree of disorder of the particles increases, which is in accordance with previous studies (e.g., [9] and references therein) that considered only isotropic dispersion. In addition, the simulations discussed previously demonstrate that this effect is more important for simulations that include anisotropic dispersion than for those that include only isotropic dispersion. However, to a certain extent, the loss of accuracy of the numerical solution can be controlled by using larger ratios between smoothing length or core size to average particle spacing. For the set of simulations analyzed, the PSE method proved to be less sensitive to particle disorder than the SPH method. Previous studies [6,9] demonstrated that the periodic remeshing of particles can help control the loss of accuracy of particle formulations due to the particle disorder caused by nonuniform flow velocity fields. Our numerical results seems to indicate that using a remeshing step is likely beneficial in simulations that consider tensorial dispersion. However, one could argue that the loss of accuracy of the particle methods for isotropic dispersion or scalar diffusion is less important; thus, the benefits of remeshing could be counterbalanced by the additional computational cost and artificial diffusion that it introduces. Yet, further studies are required to prove this hypothesis.

ACKNOWLEDGEMENTS

The contribution of the first author was funded by the Fondap-Conicyt Project 15090013.

REFERENCES

1. Bear J. *Dynamics of Fluids in Porous Media*. Dover: New York, 1988.
2. Kinzelbach W. The random walk method in pollutant transport simulation. In *Groundwater Flow and Quality Modelling*, Custodio E, Gurgui A, Lobo JP (eds). D. Reidel Publishing Company: Dordrecht, Holland, 1988; 227–246.
3. Degond P, Mas-Gallic S. The weighted particle method for convection–diffusion equations. Part 1: The case of an isotropic viscosity. *Mathematics of Computation* 1989; **53**(188):485–507.
4. Cleary PW, Monaghan JJ. Conduction modelling using smoothed particle hydrodynamics. *Journal of Computational Physics* 1999; **148**(1):227–264.
5. Eldredge JD, Leonard A, Colonius T. A general deterministic treatment of derivatives in particle methods. *Journal of Computational Physics* 2002; **180**(2):686–709.
6. Zimmermann S, Koumoutsakos P, Kinzelbach W. Simulation of pollutant transport using a particle method. *Journal of Computational Physics* 2001; **173**:322–347.

DOI: 10.1002/fld

7. Herrera P, Massabo M, Beckie R. A meshless method to simulate solute transport in heterogeneous porous media. *Advances in Water Resources* 2009; **32**:413–429.
8. Degond P, Mas-Gallic S. The weighted particle method for convection–diffusion equations. II: the anisotropic case. *Mathematics of Computation* 1989; **53**:485–508.
9. Chaniotis AK, Poulikakos D, Koumoutsakos P. Remeshed smoothed particle hydrodynamics for the simulation of viscous and heat conducting flows. *Journal of Computational Physics* 2002; **182**:67–90.
10. Crumpton PI, Shaw GJ, Ware AF. Discretisation and multigrid solution of elliptic equations with mixed derivative terms and strongly discontinuous coefficients. *Journal of Computational Physics* 1995; **116**(2):343–358.
11. Le Potier C. Finite volume monotone scheme for highly anisotropic diffusion operators on unstructured triangular meshes. *Comptes Rendus Mathématique* 2005; **341**(12):787–792.
12. Nordbotten JM, Aavatsmark I. Monotonicity conditions for control volume methods on uniform parallelogram grids in homogeneous media. *Computational Geosciences* 2005; **9**(1):61–72.
13. Mlacnik MJ, Durlofsky LJ. Unstructured grid optimization for improved monotonicity of discrete solutions of elliptic equations with highly anisotropic coefficients. *Journal of Computational Physics* 2006; **216**(1):337–361.
14. Yuan G, Sheng Z. Monotone finite volume schemes for diffusion equations on polygonal meshes. *Journal of Computational Physics* 2008; **227**(12):6288–6312.
15. Edwards MG, Zheng H. A quasi-positive family of continuous Darcy-flux finite-volume schemes with full pressure support. *Journal of Computational Physics* 2008; **227**(22):9333–9364.
16. Lipnikov K, Svyatskiy D, Vassilevski Y. Interpolation-free monotone finite volume method for diffusion equations on polygonal meshes. *Journal of Computational Physics* 2009; **228**(3):703–716.
17. Pollock D. Semianalytical computation of path lines for finite-difference models. *Ground Water* 1988; **26**(6): 743–750.
18. Bensabat J, Zhou QL, Bear J. An adaptive pathline-based particle tracking algorithm for the Eulerian–Lagrangian method. *Advances in Water Resources* 2000; **23**(4):383–397.
19. Gingold RA, Monaghan JJ. Smoothed particle hydrodynamics: theory and application to non-spherical stars. *Monthly Notices of the Royal Astronomical Society* 1977; **181**:375–389.
20. Lucy LB. A numerical approach to the testing of the fission hypothesis. *Astronomical Journal* 1977; **82**:1013–1024.
21. Monaghan JJ. Smoothed particle hydrodynamics. *Annual Review of Astronomy and Astrophysics* 1992; **30**:543–574.
22. Jubelgas M, Springel V, Dolag K. Thermal conduction in cosmological SPH simulations. *Monthly Notices of the Royal Astronomical Society* 2004; **351**:423–435.
23. Español P, Revenga M. Smoothed dissipative particle dynamics. *Physical Review E* 2003; **67**(2):026705–12.
24. Monaghan JJ. Smoothed particle hydrodynamics. *Reports on Progress in Physics* 2005; **68**(8):1703–1759.
25. Tartakovsky AM, Meakin P. A smoothed particle hydrodynamics model for miscible flow in three-dimensional fractures and two-dimensional Rayleigh–Taylor instability. *Journal of Computational Physics* 2005; **207**:610–624.
26. Herrera P, Valocchi A. Positive solution of two-dimensional solute transport in heterogeneous aquifers. *Ground Water* 2006; **44**(6):803–813.
27. Nakshatrala KB, Valocchi AJ. Non-negative mixed finite element formulations for a tensorial diffusion equation. *Journal of Computational Physics* 2009; **228**(18):6726–6752.
28. Jameson A. Positive schemes and shock modelling for compressible flows. *International Journal for Numerical Methods in Fluids* 1995; **20**.
29. Kuzmin D, Turek S. Flux correction tools for finite elements. *Journal of Computational Physics* 2002; **175**:525–558.
30. Zheng C, Bennet G. *Applied Contaminant Transport Modelling: Theory and Practice*. Van Nostrand Reinhold: New York, 1995.
31. Beaudoin A, Huberson S, Rivoalen E. Simulation of anisotropic diffusion by means of a diffusion velocity method. *Journal of Computational Physics* 2003; **186**(1):122–135.
32. Javandel I, Doughty C, Tsang C. F. *Groundwater Transport: Handbook of Mathematical Models*, Water Resources Monograph 10. American Geophysical Union: Washington, D.C., 1984.
33. Welton W. Two-dimensional PDF/SPH simulations of compressible turbulent flows. *Journal of Computational Physics* 1998; **139**:410–443.
34. Price DJ. Magnetic Fields in Astrophysics. *PhD thesis*, Institute of Astronomy, University of Cambridge, 2004.

DOI: 10.1002/fld